THE ASTROPHYSICAL JOURNAL, 449:567–575, 1995 August 20

SPECTRAL VARIABILITY OF THE X-RAY–BRIGHT BL LACERTAE OBJECT PKS 2005−489

RITA M. SAMBRUNA
Space Telescope Science Institute, 3700 San Martin Drive, Baltimore, MD 21218; sambruna@stsci.edu
C. MEGAN URRY
Space Telescope Science Institute, 3700 San Martin Drive, Baltimore, MD 21218
GABRIELE GHISELLINI
Osservatorio Astronomico di Torino, Strada Osservatorio 20, 10025 Pino Torinese, Italy
AND
LAURA MARASCHI
Dipartimento di Fisica, via Dodecaneso 33, 16146 Genova, Italy
Received 1994 November 3; accepted 1995 March 3

ABSTRACT

Two deep *ROSAT* PSPC observations of the X-ray–bright BL Lac object PKS 2005−489 have yielded high signal-to-noise spectra with a total of 18,900 and 31,000 counts. The 0.2–2.0 keV spectrum is rather steep, with a photon index around 3.0 at both epochs. The X-ray flux decreased by a factor of ≈ 2 in 6 months, accompanied by a steepening of the spectrum. Analysis of the broadband energy distribution shows that the continuum emission of PKS 2005−489 peaks at $\approx 10^{16}$ Hz and that spectral variability is greater above the peak. The application of synchrotron self-Compton models indicates that large magnetic energy densities dominate the emission region in PKS 2005−489 and that the observed variability may be the result of a variable electron energy and density. The models predict the largest variability in the γ-ray band, where the source was recently detected by the *Gamma Ray Observatory* (*GRO*).

Subject headings: BL Lacertae objects: individual (PKS 2005−489) — gamma rays: theory — radiation mechanisms: nonthermal — X-rays: galaxies

1. INTRODUCTION

PKS 2005−489 is a BL Lac object in the complete sample drawn from the 1 Jy radio catalog (Stickel et al. 1991; Kühr et al. 1981). It was discovered in the Parkes 2.7 GHz survey (Wall, Shimmins, & Bolton 1975), classified first as an N galaxy (Savage, Bolton, & Wright 1977), and subsequently identified as a BL Lac object on the basis of the bright star–like nucleus, flat radio spectrum, and featureless optical continuum (Wall et al. 1986, and references therein). It is one of the brightest BL Lac objects at all observed frequencies. The maximum recorded value of the polarization of its optical light is 2%, while most BL Lac objects of the 1 Jy sample exhibit higher values (Stickel, Fried, & Kühr 1993). Weak narrow emission lines were detected during a low state of the optical continuum allowing the determination of the redshift, $z = 0.071$ (Falomo et al. 1987). Together with several other BL Lac objects, PKS 2005−489 is one of the few extragalactic sources detected in the EUV band (Marshall, Fruscione, & Carone 1995; Fruscione 1995). The object belongs to a cluster of galaxies (Pesce et al. 1994).

PKS 2005−489 is by definition a radio-selected BL Lac object (RBL). However, on the basis of its X-ray-to-radio flux ratio, it would be classified as an "X-ray–strong" or "radio-weak" or "XBL-like" object (Ledden & O'Dell 1985; Maraschi et al. 1986; Giommi & Padovani 1994), the latter term meaning that its radio-to-X-ray energy distribution is similar to those of X-ray selected BL Lac objects (XBLs). Together with several RBLs of the 1 Jy sample, PKS 2005−489 was recently detected at ~ 1 GeV by the EGRET experiment of the *Compton Gamma Ray Observatory* (*CGRO*), with a significance of 4.3 σ (*CGRO* electronic database).

In X-rays, PKS 2005−489 was observed five times with the *EXOSAT* satellite, showing large flux variations and correlated changes in spectral shape (Wall et al. 1986; Giommi et al. 1990); the 0.1–10 keV spectrum steepens with fading intensity, a behavior often displayed by other XBLs (Sambruna et al. 1994a, b). Two long exposures were obtained with the *ROSAT* Position Sensitive Proportional Counter (PSPC) in 0.1–2.4 keV, allowing the study of the soft X-ray spectrum and its variability.

Here we present a detailed analysis of the two archival *ROSAT* PSPC observations of PKS 2005−489, as part of an ongoing study of the soft X-ray properties of the 1 Jy RBLs observed with *ROSAT* (Urry et al. 1995). The X-ray spectral variability is interpreted in the context of inhomogeneous relativistic jet models.

2. *ROSAT* OBSERVATIONS

2.1. *Analysis Procedure*

PKS 2005−489 was observed in pointed mode with the *ROSAT* PSPC on two occasions in 1992. On both dates the exposures were rather long (>10,000 s), yielding a total of $\sim$31,000 and 18,900 counts, respectively, in the 0.1–2.4 keV energy range. In both images, the object was positioned in the center of the field, and the *ROSAT* coordinates are consistent with the optical-radio position. The source image appears blurred as an effect of the scattering of the softest ($\lesssim 0.15$ keV) photons, which is known as the "ghost-image" problem (see "The *ROSAT* Users' Handbook" [Briel et al. 1994]). The observed radial profiles are in good agreement with the model point spread function, indicating that no extended emission is present.

The source photons were collected in a circle of radius 2.5 centered on the source position. This radius is large enough to

TABLE 1

LOG OF THE *ROSAT* OBSERVATIONS OF PKS 2005−489

Date	Exposure (s)	Image Number	Counts per Second[a]
1992 Apr 27–29	10,487[b]	WP700488	2.56 ± 0.02
1992 Oct 28–Nov 1.....	11,462	WP701057	1.40 ± 0.01

[a] In the 0.2–2.0 keV energy range.
[b] Effective exposure after 1000 s were cut for variable background.

collect also the ghost-image photons. The background was evaluated in an annulus around the source with inner and outer radii 3′ and 7′. A source located ∼6′ from the BL Lac object, coinciding with an F8 star, was excluded from the background region. As listed in the WGA catalog (White, Giommi, & Angelini 1994), the other sources present in the field of PKS 2005−489 are either too faint ($\lesssim$0.002 counts s^{-1}) or too distant (>7′) to affect the analysis. During the April observation the background light curve showed anomalous trends and several flares; these times were cut in the further analysis, yielding an effective exposure time of 10,487 s.

The net count rates of PKS 2005−489 in the 0.2–2.0 keV energy range are reported in Table 1. During the November observation the source was fainter than in April, with a drop of the count rate of a factor ∼1.8 in ∼6 months. PKS 2005−489 was detected during the *ROSAT* All-Sky Survey (RASS) with an intensity of 2.61 ± 0.09 counts s^{-1} on the 0.1–2.4 keV range (R. Petre, private communication), comparable to the brighter April observation.

Time variability of the X-ray emission within each of the two observations was studied using the Kolmogorov-Smirnov (K-S) and χ^2 tests. We applied both tests to the full light curves and to data accumulated on individual orbits. Because of the wobble of the satellite, the light curves were binned at $\gtrsim$400 s. No variability was detected, according to both the χ^2 and K-S tests.

The spectra were extracted on the full 256 channel range. In order to have Gaussian errors, the spectra were rebinned so that each bin contained at least 50 photons and the channel range was restricted to where the spectral response is best known (0.2–2.0 keV). Spectral fits were performed using XSPEC, with the matrix recommended for data taken in low-gain mode (appropriate to observations after 1991 October 14), i.e., the pspcb93jan12 matrix. Some residual uncertainties remain, so in order not to overestimate possible narrow features, a systematic 2% error was added to the data.

2.2. *Fits to the ROSAT Spectrum of PKS 2005−489*

The spectra were fitted with a single power-law model, modified at low energies by absorption due to cold gas. The fits were performed both allowing the absorbing column density N_H to vary and fixing N_H to the Galactic value 4.6×10^{20} cm^{-2}. The latter value was obtained from an interpolation of the distribution of the Galactic N_H from the Stark et al. (1992) survey as a function of the Galactic latitude, following Giommi et al. (1990; P. Giommi, private communication), and the rms uncertainty is 3×10^{20} cm^{-2} (Urry et al. 1995). The recent detection of PKS 2005−489 in the EUV range suggests that the Galactic N_H is probably $\sim 3 \times 10^{20}$ cm^{-2} and should not exceed 6×10^{20} cm^{-2} (H. Marshall, private communication).

The results of the power-law fits are reported in Table 2. We quote the photon index (Γ) in columns (3) and (6), the fitted column densities (N_H) in column (5), and the reduced χ^2 values per degrees of freedom (χ^2_r/dof) in columns (4) and (7). Also reported in the Table are the flux densities at 1 keV (col. [2]), from the fits with fixed N_H. The spectral parameters are determined at 90% confidence for two interesting parameters ($\Delta\chi^2 = 4.6$). For the fits with fixed N_H, the normalization was considered an interesting parameter because it determines the quoted 1 keV flux density.

The χ^2_r values reported in Table 2 show that the fits with a single power law and fixed absorption are clearly unacceptable in both observations. Leaving N_H free to vary yields acceptable fits, with quite steep photon indices (∼3.0) in both cases. Figure 1 shows the χ^2 confidence contours for the latter fits. Both observations are consistent with the same value of the photon index; in effect, the spectrum steepens in a way that can be described by decreasing N_H and normalization. A steeper spectrum ($\Gamma = 3.46 \pm 0.28$), with higher $N_H = (5.0 \pm 1.3) \times 10^{20}$ cm^{-2}, was derived by Brinkmann & Siebert (1994) from the RASS data.

The residuals of the fixed- and free-N_H models are plotted in Figures 2*a*–2*b* for the April data and in Figures 2*c*–2*d* for the November spectrum. In both fits with fixed absorption (panels [a] and [c]), the most prominent feature is a deficiency of photons centered at ∼0.5 keV, significant at greater than 99% confidence, according to an *F*-test (Table 3). However, the feature significance depends strongly on the value of the fixed absorption. For $N_H > 4.6 \times 10^{20}$ cm^{-2}, the feature is deepened, while for lower Galactic absorption its significance becomes negligible. In fact, if the absorption is left free to vary (panels [b], and [d]), the significance of the feature drops to a negligible value in both observations (Table 3).

One of the pending problems concerning the calibration of the PSPC spectral response is represented by the temporal gain shifts, which can create spurious features in the observed spectra. In § 2.3 we describe our simulations of the effects of the PSPC gain shifts. Here we note that the matrix used to analyze the data of PKS 2005−489, pspcb93jan12, was obtained by fudging the "high-gain" response (pspcb92mar11) with the data of Mrk 421, observed by *ROSAT* in a long exposure in 1992 May, i.e., between the two observations of PKS 2005−489 but closer to the first one. If the gain temporal variations are small on a timescale of a few months, the

TABLE 2

SINGLE POWER-LAW SPECTRAL FITS

		N_H FIXED		N_H FREE		
EPOCH (1)	$F_{1\,keV}$ (μJy) (2)	Γ (3)	χ^2_r/dof (4)	N_H ($\times 10^{20}$ cm^{-2}) (5)	Γ (6)	χ^2_r/dof (7)
1992 Apr	5.05 ± 0.10	3.08 ± 0.02	2.00/35	4.07 ± 0.21	2.92 ± 0.07	1.21/34
1992 Oct–Nov.....	2.70 ± 0.08	3.25 ± 0.03	3.36/35	3.47 ± 0.26	2.88 ± 0.09	1.08/34

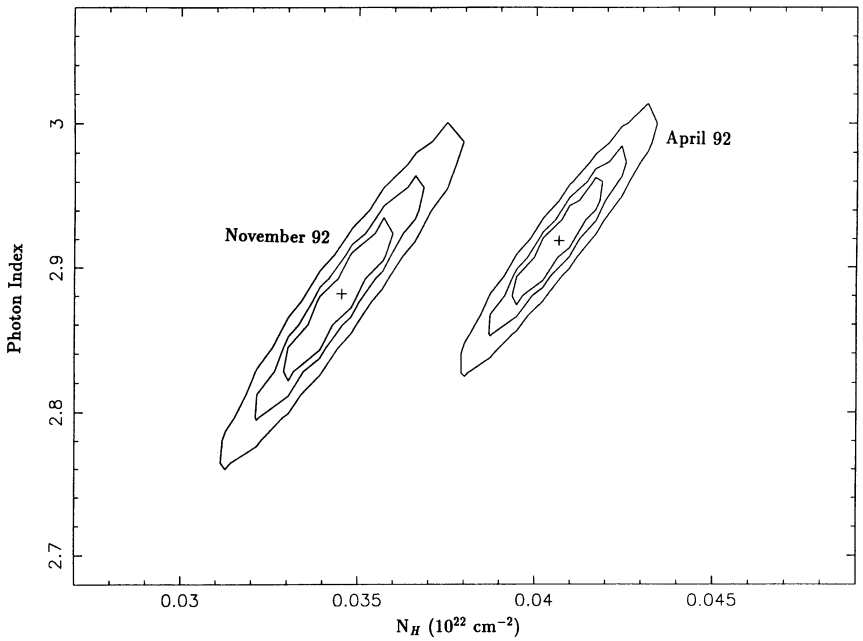

FIG. 1.—The χ^2 confidence contours for the power-law fits to the *ROSAT* observations of PKS 2005−489. The abscissa is the absorption column density in 10^{22} cm^{-2}, the ordinate is the photon index. The best-fit (*cross*) and the 68%, 90%, and 99% confidence levels are plotted.

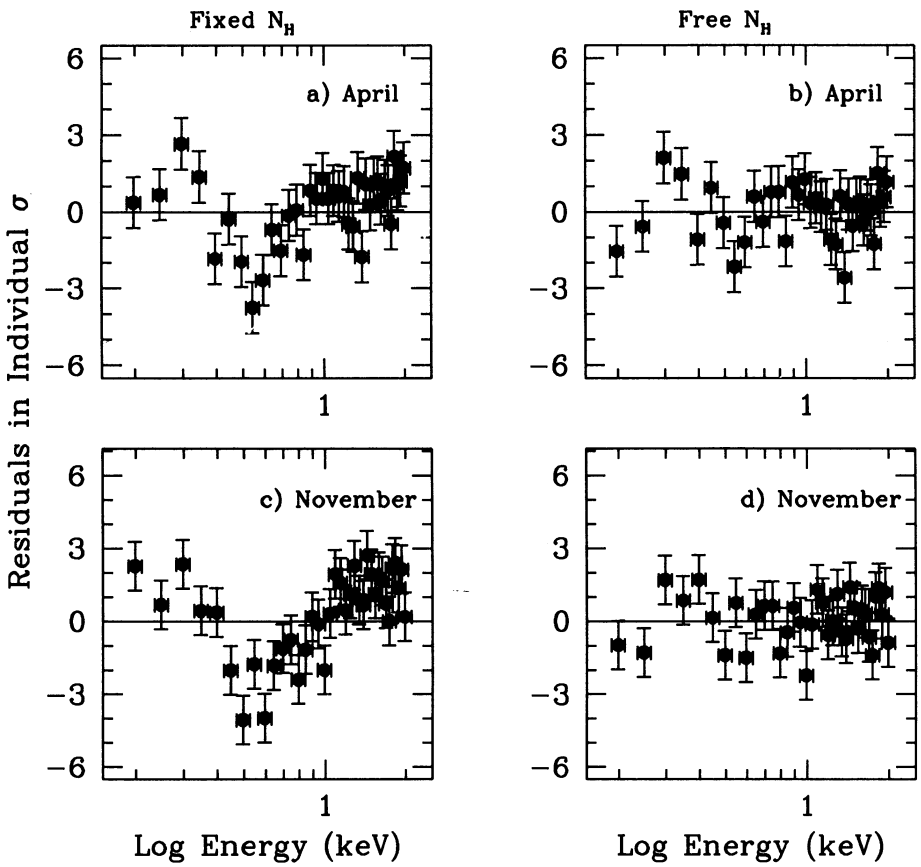

FIG. 2.—Residuals of the fit with the single power law plus low-energy absorption model to the *ROSAT* data of PKS 2005−489. Residuals of the fits with $N_H = 4.6 \times 10^{20}$ cm^{-2} for (*a*) April and (*c*) November data. An absorption feature, significant at greater than 99% according to an *F*-test, is present at 0.5 keV in both observations. Fits with free N_H to (*b*) April and (*d*) November data. The residuals of both data sets appear featureless.

TABLE 3

POWER-LAW PLUS EDGE SPECTRAL FITS

	$N_H = 4.6 \times 10^{20}$ cm^{-2}				N_H FREE				
EPOCH (1)	Γ (2)	E(keV) (3)	τ (4)	χ_r^2/dof (5)	$N_H(10^{20}$ cm$^{-2})$ (6)	Γ (7)	E_L(keV) (8)	τ (9)	χ_r^2/dof (10)
1992 Apr	3.06 ± 0.03	$0.455^{+0.074}_{-0.177}$	$0.309^{+1.042}_{-0.137}$	0.85/33	$4.85^{+0.65}_{-0.68}$	$3.00^{+0.12}_{-0.06}$	$0.451^{+0.069}_{-0.17}$	$0.393^{+0.746}_{-0.313}$	1.10/32
1992 Oct–Nov.....	$3.19^{+0.05}_{-0.04}$	$0.486^{+0.056}_{-0.173}$	$0.565^{+0.198}_{-0.187}$	0.87/33	$3.90^{+0.1}_{-0.6}$	~ 3.0	~ 0.5	$0.3(<0.7)$	1.04/32

93jan12 matrix should be appropriate to fit the *ROSAT* data of PKS 2005−489 and gain shifts should not introduce absorption features.

We did explore the effect of fitting the spectra of PKS 2005−489 with the inappropriate 92mar11 matrix, which corresponds to a different gain setting than the 93jan12 matrix. This changes considerably the energy and depth of the fitted absorption feature when the Galactic N_H is fixed (as expected). In the fits with the 92mar11 matrix, E_L is determined around 0.28 keV, the energy of the carbon edge, one of the primary constituents of the instrument window, and the feature is deepened ($\tau \sim 2$–3). The simulations described in § 2.3 show that gain shifts even smaller than those appropriate to the 93jan12 matrix can create residuals similar to those observed in PKS 2005−489.

We conclude that, at the present level of knowledge of the Galactic absorption and of the instrumental uncertainties, the *ROSAT* spectrum of PKS 2005−489 appears well described by a single power-law model with steep photon index ($\Gamma \sim 3.0$) and a column density ~ 3–4×10^{20} cm^{-2}.

2.2.1. *Upper Limits for Other Features*

Absorption features from highly ionized gas have been seen in other BL Lac objects. An absorption feature was seen at 0.6 keV in the X-ray spectrum of the bright BL Lac object PKS 2155−304 taken with the *Einstein* Objective Grating Spectrometer (Canizares & Kruper 1984). The redshift of the source favored an interpretation as the resonant Lyα line of O VIII ($E_{rest} = 0.654$ keV; Canizares & Kruper 1984; Krolik et al. 1985). A feature at 0.55 keV was detected in the BBXRT spectrum of PKS 2155−304 and best-fitted by a broken power law plus edge model, with the energy of the edge at ~ 0.506 keV and $\tau \sim 1.1$ (Madejski et al. 1995).

We can set upper limits on the strength of absorption features of the same kind as in the OGS and BBXRT spectra of PKS 2155−304 in the *ROSAT* data of PKS 2005−489. We modeled the oxygen resonant line with a notch model, with fixed energy 0.61 keV and covering fraction 1; the fit to the data with this model yielded a negligible value of the line width, $\Delta E \lesssim 0.02$ keV, in both spectra, or, fixing the width at 0.1 keV, negligible covering fraction, $\lesssim 0.2$. For the BBXRT feature, a power law plus edge model yielded $\tau = 0.15$–0.25.

2.2.2. *Upper Limits for the X-Ray Luminosity of the Associated Cluster*

The softness of the spectra derived in both April and November observations implies that any contribution to the soft X-ray emission by the hot gas of the cluster associated with PKS 2005−489 (Pesce, Falomo, & Treves 1994) should be negligible; in fact, fitting the data with a two-component model (power law plus thermal bremsstrahlung) does not yield an improved fit.

We can estimate an upper limit to the X-ray luminosity of the cluster. Assuming a power law with $\Gamma = 3$ for the BL Lac object, a thermal bremsstrahlung with temperature $kT = 5$ keV for the cluster (an average value derived from *EXOSAT* measurements; Edge & Stewart 1991), and $N_H = 4.6 \times 10^{20}$ cm^{-2}, the maximum luminosity a cluster could have and not be detected in our data is $L_x(0.2$–2.0 keV$) \approx 8 \times 10^{43}$ ergs s^{-1}, a factor of 4 fainter than the BL Lac object and typical of poor clusters (e.g., Price et al. 1991).

2.3. *Simulations of the Effects of the PSPC Gain Shifts*

The temporal variations of the PSPC gain are among the pending problems concerning the calibration of the spectral response. A gain shift assigns systematically different channels to incoming photons of a given energy, with the net result that the spectrum is shifted forward or backward in the detector sensitivity range. When not compensated for in the detector response matrix, this may lead to the presence of localized zero or low-counts channels, which appear as spurious features.

A proper test of this effect would be to simulate data with a response matrix appropriate to one gain setting, and then analyze it with the matrix appropriate to another gain (test A). An artificial but qualitatively equivalent procedure (test B), which explores more than two gain settings, is to simulate data with one matrix, shift it artificially by a fixed number of channels (this ignores effects of nonlinearity and so on), and compare the simulated spectrum with the real data. Both tests are described below in turn. The simulations are normalized to the count rate of the April observation of PKS 2005−489 and were created with a power-law model with $\Gamma = 3.0$ and $N_H = 4.6 \times 10^{20}$ cm^{-2}.

a) Inappropriate instrumental response matrix (test A).—We have at our disposal the two matrices corresponding to the setting obtained in "low-gain" mode (pspcb93jan12) and in "high-gain" mode (pspcb92mar11). Single–power-law 256 channel spectra were simulated with the command FAKEIT within XSPEC using the two matrices in turn and rebinned in the way described above for the observed data. The spectrum faked with the 92mar11 matrix was then analyzed with the 93jan12 matrix and vice versa. The residuals of the single power law plus Galactic N_H model are shown in Figure 3 for the two cases, respectively.

From Figure 3 it can be seen that, in the case of the spectrum created with the "high-gain" matrix (panel a) an absorption feature is created at $E_L \sim 0.6$ keV, with a small optical depth, $\tau \sim 0.13$, and emission at lower energies. In the spectrum simulated with the "low-gain" response (panel b), a deeper feature ($\tau \sim 1.5$) appears at ~ 0.26 keV, close to the instrumental carbon edge. In other words, if the gain decreased substantially from the 93jan12 level during the PKS 2005−489 observations, our use of the high-gain matrix to analyze the data could create a spurious absorption feature but at a lower energy than observed.

b) Artificial gain shifts (test B).—A single power-law spectrum with no absoption features was simulated using the 93jan12 matrix, and the 256 channel spectrum was rebinned as

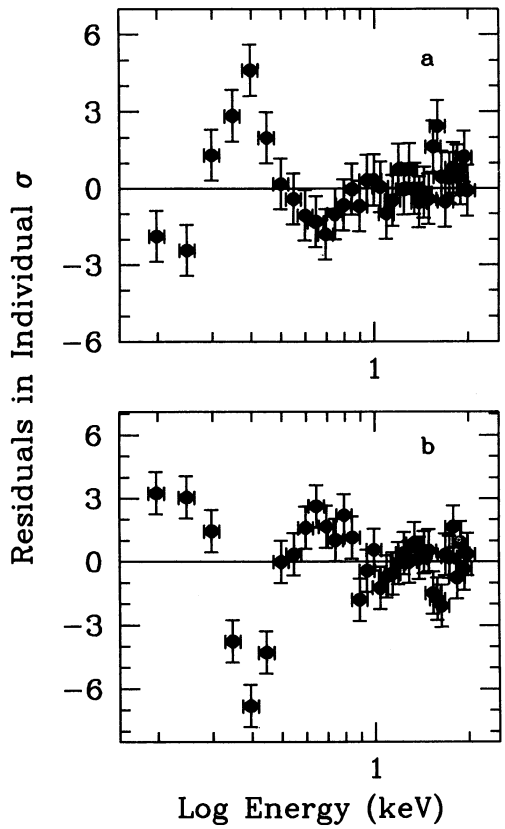

FIG. 3.—Results from the simulations of the PSPC gain shifts (test A; see text). (*a*) Residuals of the fit with the single power law plus Galactic absorption model to the spectrum simulated with the 92mar11 matrix and analyzed with the 93jan12 matrix. A negligible ($\tau \sim 0.13$) feature is created at 0.6 keV, while a prominent emission structure appears at 0.4 keV. (*b*) Same as (*a*), but for the spectrum simulated with the 93jan12 matrix and analyzed with the 92jan11 matrix. A deep ($\tau \sim 1.5$) absorption feature shows up at 0.26 keV, close to the instrumental carbon edge.

in the case of the real data. The simulated spectrum was artificially shifted forward and backward, toward higher and lower gains, respectively, by adding zero channels on the top or the bottom of the ASCII file. Panels a and b of Figure 4 show the residuals of the power-law model fit to the spectra shifted forward by six channels and backward by two channels, respectively, they represent cases analogous to those in Figure 3.

Panel c of Figure 4 shows the difference between the observed data and the simulated (unshifted) power law; an absorption feature is effectively present in the real data at 0.5 keV, together with an excess at lower energies. However, both the feature and the excess can be reproduced with a small (1 channel) shift forward, as shown in panel d of Figure 4.

3. THE BROADBAND ENERGY DISTRIBUTION OF PKS 2005−489

3.1. *The Data*

In the following we discuss the high-energy emission of PKS 2005−489 in relation to its overall broadband energy distribution (BBED). Unfortunately, no data simultaneous to either the *ROSAT* or the γ-ray observations are available at other frequencies. A representative BBED from radio to X-rays was therefore derived from published flux densities (a literature search in the period 1900–1994 made use of the electronic database NED). With the exception of the radio measurements, all the fluxes were actually obtained in the last 15 years. Radio flux densities at 0.41, 2.7, and 5.0 GHz were obtained by Large et al. (1981), Wall et al. (1975), and Kühr et al. (1981). *JHKL* and *V* photometry was performed by Bersanelli et al. (1992), Falomo et al. (1993), and Wall et al. (1986, and references therein). PKS 2005−489 was detected by *IRAS* at 12, 25, 60, and 100 μm (Impey & Neugebauer 1988). Data in the UV band are reported in the compilation of Edelson et al. (1992).

X-ray observations prior to those from *ROSAT* ones were obtained with the *EXOSAT* satellite in the 0.1–10 keV range, at five different epochs in the period 1984–1985 (Sambruna et al. 1994b). The spectral index was observed to vary from $\Gamma = 2.62 \pm 0.02$ in the highest state to $\Gamma = 3.20^{+0.20}_{-0.14}$ in the lowest state. The highest intensity state measured with *EXOSAT* is the brightest state observed so far in X-rays for this source, with $F_{1\,\mathrm{keV}} \sim 40$ μJy. The lowest *EXOSAT* state is very close in both slope and normalization to the 1992 November *ROSAT* observation.

Figure 5 shows the BBEDs obtained by plotting at each frequency the maximum (*filled circles*) and minimum (*open circles*) "historical" flux density. In X-rays, spectra corresponding to the brightest *EXOSAT* state and to the faintest state measured with both *ROSAT* and EXOSAT are plotted. This procedure yields two BBEDs which may be taken to represent the continuum energy distribution in a "high" and "low" state, respectively. The γ-ray flux corresponding to the marginal (4.3 σ) detection, $\sim 3.0 \times 10^{-11}$ Jy, is also shown together with the highest 2 σ upper limit obtained on a different occasion (CGRO electronic database).

Despite the nonsimultaneity of the data plotted in Figure 5, the BBED of PKS 2005−489 shows some clear trends. The power per decade rises continuously from the radio to the IR-optical-UV bands, reaching a peak in the soft X-ray band. This is typical of XBL-like BL Lac objects (Giommi, Ansari, & Micol 1995). Following the peak, the power per decade decreases in the medium X-ray range, but the γ-ray data imply a second rise and a second peak.

Note that the flux variations are largest at frequencies *higher* than 10^{16} Hz, which corresponds to the peak of the power per decade, while at lower energies the flux variability is less dramatic (Fig. 5). In the X-ray band there seems to be a regular trend in the spectral variability, with a softer spectrum in the fainter state, as seen in other BL Lac objects (Giommi et al. 1990; Sembay et al. 1993; George, Warwick, & Bromage 1988). This was previously noted within the *EXOSAT* data (Sambruna et al. 1994a) and is supported by the *ROSAT* data (see above).

3.2. *Interpretation*

There is general consensus that the multifrequency continuum from blazars at least up to the UV band is due to synchrotron radiation from high-energy electrons within a relativistic jet (e.g., Königl 1989). The "curved" shape of the continuum may be due to the superposition of different emission regions with different particle spectra (inhomogeneous models), or to curvature of the particle spectrum of a single emission region, or both. Inhomogeneity is probably responsible for the flat radio spectra, where individual components are optically thick (Ghisellini, Maraschi, & Treves 1985).

In the case of PKS 2005−489, the steepness of the X-ray spectrum and its variability behavior (steepening of the spectrum with decreasing intensity, but always smoothly connect-

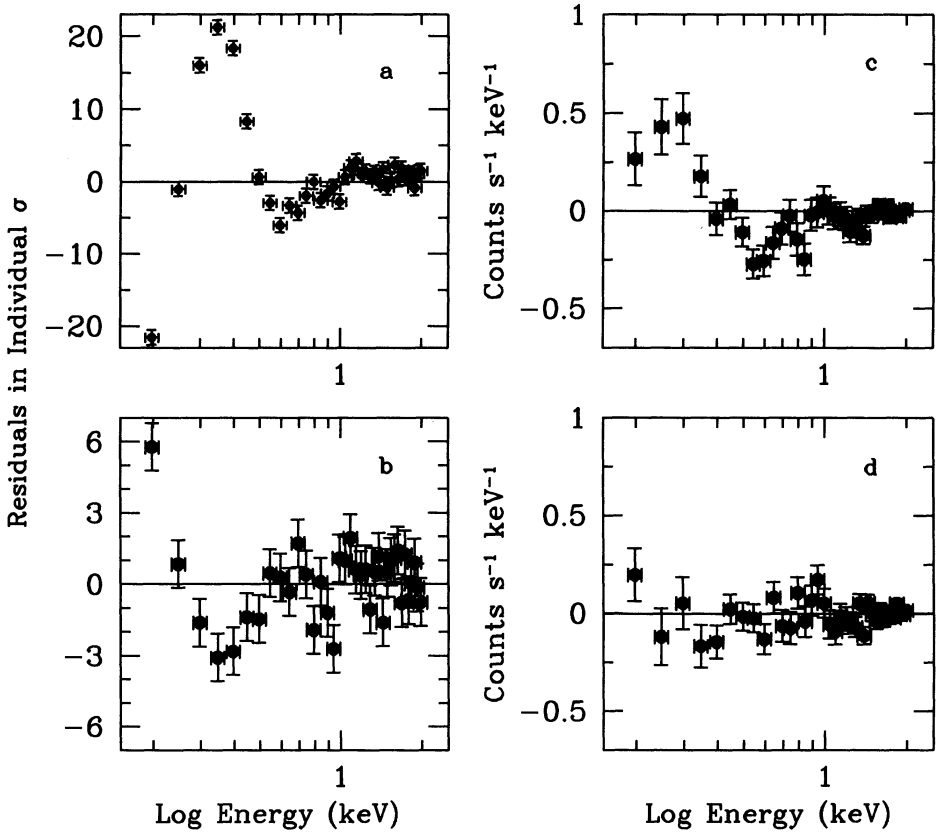

FIG. 4.—Results from the simulations of the PSPC gain shifts (test B; see text). A single power-law was simulated and shifted both forward, toward higher gains, and backward (lower gains). Residuals of the single power-law model for the simulated spectrum shifted by (*a*) six channels toward higher gains and by (*b*) two channels toward lower gains. These shifts create situations similar to those in panels a and b of Figure 3 respectively. (*c*) The simulated unshifted power law is subtracted from the true April data. A feature in the true data is visible at 0.5 keV, together with excess emission at lower energies. (*d*) Difference between the April data and the simulated spectrum shifted forward by one channel. A small gain shift can produce the residuals observed in the true data.

ing with the optical-UV) suggest that the X-ray emission may also have a synchrotron origin. The observed spectral variability can be interpreted within homogeneous or inhomogeneous models as discussed below.

The γ-rays may be produced via the inverse Compton process by the same high-energy electrons responsible for the synchrotron continuum. Suggested origins for the seed photons include the synchrotron photons themselves (synchrotron self-Compton, SSC; e.g., Maraschi, Ghisellini, & Celotti 1992), UV photons coming from a nearby accretion disk (Dermer, Schlickeiser, & Mastichiadis 1992), or from the broad-line region (Sikora, Begelman, & Rees 1994). Here we discuss the SSC model (see also Ghisellini & Maraschi 1994), considering first the homogeneous case and then a more realistic inhomogeneous jet model.

3.3. *Homogeneous Synchrotron Self-Compton Model*

We can derive order of magnitude estimates of the magnetic field and the size of the γ-ray–emitting region of PKS 2005−489 from a simple homogeneous SSC model. We assume that the synchrotron component is responsible of the UV peak in the BBED (at $\nu_s \sim 10^{16}$ Hz), and that the corresponding peak due to the self-Compton process is approximately at the observed γ-ray energies (at $\nu_c \sim 10^{23}$ Hz). The ratio of these two energies is approximately equal to the square of the Lorentz factor of the emitting electrons, so $\gamma \sim 3 \times 10^3$. To produce synchrotron photons of observed frequency $\nu_s = 10^{16}\nu_{s,16}$ Hz with this electron Lorentz factor, the magnetic field must be $B \sim 360\nu_{s,16}^2/(\delta\nu_{c,23})$ G, where δ is the beaming factor and $\nu_c = 10^{23}\nu_{c,23}$ Hz.

From Figure 5 one finds that the IR-optical UV flux (integrated over frequency) of the "high" state is approximately 10 times the observed flux above 100 MeV. If the former is due to the synchrotron process, and the latter to self-Compton scattering, one finds $U_B \sim 10U_{\rm rad}$. Therefore we have

$$10\,\frac{L_{\rm syn}}{4\pi R^2 c\delta^4} = \frac{B^2}{8\pi}\,, \tag{1}$$

where $L_{\rm syn} = 10^{46}L_{\rm syn,46}$ ergs s^{-1} is the observed synchrotron luminosity. Equation (1) implies

$$R \sim 7.2 \times 10^{15}\,\frac{L_{\rm syn,46}^{1/2}}{\delta}\,\frac{\nu_{c,23}}{\nu_{s,16}^2}\ {\rm cm}\,. \tag{2}$$

The corresponding minimum variability timescale $t_{\rm var} = R/(c\delta) \sim 2.8L_{\rm syn,46}\,\nu_{c,23}/(\delta\nu_{s,16})^2$ days. We note that rapid variations have indeed been observed in the X-rays, with $t_{\rm var} \sim$ 2 hr (Giommi et al. 1990), thus suggesting $\delta \sim 6$. This is consistent with a lower limit on the beaming factor, $\delta > 3.4$, derived by requiring the source to be transparent to γ-rays (Dondi & Ghisellini 1995).

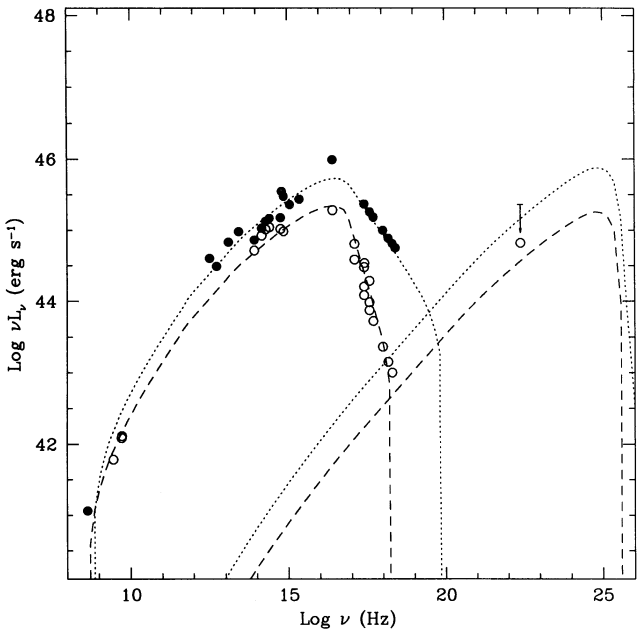

FIG. 5.—Broadband energy distribution of PKS 2005−489. Data are taken from the literature and are not simultaneous. Maximum (*filled circles*) and minimum (*open circles*) historical fluxes are plotted from radio to UV. In X-rays the high state measured with *EXOSAT* and the low states measured with *ROSAT* and *EXOSAT* are plotted. In γ-rays, the marginal (4.3 σ) detection and the higher 2 σ upper limit measured with *CGRO* on separate occasions are plotted. Dotted and dashed lines represent the fits with the inhomogeneous relativistic jet models of Ghisellini et al. (1985) to the high and low states, respectively.

In the framework of the homogeneous SSC model, the IR to X-ray emission must be produced by a broken power-law distribution of relativistic electrons, with a break at the electron Lorentz factor γ_b. Radiation losses are severe (unless δ is unrealistically large) and are more rapid than the light crossing time, implying a continuous injection of particles. In such cases the equilibrium particle distribution, derived by a continuity equation, is found by balancing injection and losses. A broken power law can be obtained by injecting a power law of relativistic electrons of slope s above the break energy γ_b. The steady particle distribution $N(\gamma)$, will be a power law of slope 2 below γ_b, and slope $(s + 1)$ above. The observed spectral variability can then be due to a change in the injection index s, resulting in a spectral change above the break energy, but in the same slope below.

3.4. *Inhomogeneous Relativistic Jet Model*

A simple homogeneous SSC model has difficulties in accounting for the overall spectrum of PKS 2005−489 from the far-IR to the γ-rays. Furthermore, it is widely believed that in blazars most of the emission is produced in a relativistic jet pointing at the observer. We have therefore considered the inhomogeneous jet model of Ghisellini et al. (1985, hereafter GMT), where the relevant quantities (magnetic field, electron density, maximum emitted synchrotron frequency) are simple power-law functions of the distance from the apex of the jet.

The BBEDs of PKS 2005−489 in high and low states can be reproduced, as shown in Figure 5, with the parameters listed in Table 4. Because of the large number of free parameters, we did not attempt to constrain parameters individually but simply tried to obtain a reasonable fit to both BBEDs. A constant bulk Lorentz factor $\Gamma_B = 5$, a viewing angle $v = 10°$, an initial value of the magnetic field close to the estimates of the preceding section, $B_0 = 130$ or 110 G, and maximum synchrotron frequency $\nu_{max} = 1.7 \times 10^{19}$ or 4×10^{17} Hz, produce the fits to the high and low states, respectively (dotted and dashed lines in Fig. 5). In the GMT model, most of the IR to γ-ray emission is produced in the inner, parabolic zone of the jet ($R \lesssim 10^{17}$ cm). In this region the magnetic field decreases from 130 to 4 G, while the particle density stays approximately constant. The larger conical zone is responsible for the radio emission. The magnetic energy density is larger than either the particle energy density or the radiation energy density throughout the entire jet.

The slope of the soft X-rays in this model is due to the convolution of the spectra produced in each slice of the inner jet rather than to a steep electron distribution. The high and low states of the source have been reproduced decreasing the maximum energy of the electrons (via ν_{max}), and to a lesser extent increasing the electron density, while maintaining (approximately) constant the magnetic field and the other parameters of the source. This suggests that the variable slope and flux of the X-rays is due to a change in the electron distribution function in the inner part of the jet. As can be seen in Figure 5, variations in the IR-optical bands should be accompanied by corresponding simultaneous *larger* variations in γ-rays. The variability of X-rays emitted via synchrotron radiation might have a correspondence at ultra-high (TeV) γ-ray

TABLE 4

INHOMOGENEOUS JET MODELS FOR PKS 2005−489[a]

Parameter	High State	Low State	Notes
R_0	1×10^{14} cm	1×10^{14} cm	Initial radius of parabola
$R_{max,par}$	1×10^{17} cm	1×10^{17} cm	Maximum length of parabola
$R_{max,cone}$	3×10^{20} cm	3×10^{20} cm	Maximum length of cone
B_0	130 G	110 G	Magnetic field at R_0
τ_0	2.8×10^{-6}	4.5×10^{-6}	Optical depth at R_0
ν_{max}	1.7×10^{19} Hz	4×10^{17} Hz	Maximum synchrotron frequency at R_0
m	1.0	1.0	Magnetic field power-law index
n	0.20	0.50	Electron density power-law index
$\Gamma_{B,0}$	5.0	5.0	Bulk Lorentz factor (constant)
v	10°	10°	Viewing angle
K_0	4.2×10^4 cm^{-3}	6.8×10^4 cm^{-3}	e- density at R_0
δ	5.7	5.7	Doppler factor
U_r/U_B	0.92	0.25	Photon/magnetic densities at R_0
β	4.8	4.8	Predicted superluminal speed

[a] Symbols for the parameters as in Ghisellini et al. 1985.

energies where, however, the Compton scattering cross section is reduced by the Klein-Nishina limit. The models shown in Figure 5 illustrate the importance of coordinated observations in the optical-UV, X-ray, and γ-ray bands.

4. DISCUSSION

It is interesting to compare the spectral properties of PKS 2005−489 to those of other blazars. The radio to X-ray energy distribution resembles that of XBL-like BL Lac objects. In particular, PKS 2005−489 shows close similarities to Mrk 421, a prototype X-ray bright BL Lac object. In addition to the shape of the overall energy distribution, properties in common to both sources include the steepness of the X-ray spectrum, the trend of harder X-ray spectrum with higher intensity, and the detection at γ-ray energies. In fact, applying the same jet model to Mrk 421 yields physical parameters similar to those derived here for PKS 2005−489 (Maraschi, Ghisellini, & Boccasile 1994). Mrk 421 is the first (and only) extragalactic source detected at TeV energies. Note that in Figure 5 the Compton component in the spectrum of PKS 2005−489 peaks at 10^{25} Hz. Because of its proximity ($z = 0.071$), PKS 2005−489 could likely be detected at TeV energies with current sensitivities. Unfortunately this is not currently feasible, since the object is located in the southern hemisphere.

It is also interesting to compare PKS 2005−489 and 3C 279, the best-studied γ-ray–loud blazar, because for both sources we have information about high and low states. Like PKS 2005−489, the BBED of 3C 279 showed a softening of the continuum with fading intensity from IR to UV frequencies; in addition, the γ-ray power of 3C 279 was largely dominant in the high state, while it was less prominent in the low state (Maraschi et al. 1994). The two objects have different classifications, PKS 2005−489 being a BL Lac object while 3C 279 is a more luminous, superluminal quasar. For the latter object, as for many radio-selected BL Lac objects, the peak in the broadband energy distribution is between 10^{12}–10^{14} Hz (Maraschi et al. 1994; Giommi et al. 1995), much lower than in the case of PKS 2005−489. Another clear difference is that in 3C 279 the X-ray emission has a flat spectrum extrapolating smoothly to the γ-rays. Therefore, in the latter object the X-rays do not derive from the synchrotron mechanism but most likely from inverse Compton scattering.

It is interesting to note that *in both* 3C 279 and PKS 2005−489, the largest variations and the softening of the continuum with decreasing intensity occur beyond the peak in the broadband energy distribution. The two BBEDs and the spectral behaviors can be thought of as similar if one allows for a shift of $\sim$3 orders of magnitude in the frequency axis of the multifrequency spectrum. Such a shift may result from similar emission mechanisms operating in the whole blazar class but on different physical scales. The different position of the spectral break in the two BBEDs, $\nu_S \approx 10^{13}$ Hz in 3C 279 and $\approx 10^{16}$ Hz in PKS 2005−489, indicates a higher magnetic field and/or a higher particle energy in the latter source for comparable δ factors. Application of the same inhomogeneous jet model to 3C 279 (Maraschi et al. 1992, 1994) does yield a lower magnetic field, larger size, and lower particle energies. It is also interesting to note that the different magnetic field value may account for the different dominance of the γ-ray emission in the two sources if the γ-rays are produced through the SSC mechanism. The lower magnetic field value in 3C 279 may mean that Compton energy losses exceed synchrotron losses, with consequent copious production of γ-rays. A systematic analysis of the BBEDs of complete samples of blazars, for the purpose of a physical characterization of their emission properties, is in progress (Sambruna et al. 1995).

5. SUMMARY AND CONCLUSION

Two *ROSAT* PSPC pointed observations of the X-ray bright BL Lac object PKS 2005−489 show interesting spectral characterics. The 0.2–2.0 keV continuum of PKS 2005−489 is steep ($\Gamma \sim 3.0$) and extrapolates well to the faintest spectrum measured with *EXOSAT* in a harder range. The *ROSAT* data show that for the soft X-ray band, as previously found for hard X-rays, the X-ray spectrum hardens with increasing intensity.

The smooth connection of the X-ray spectrum to the optical UV continuum suggests a common synchrotron origin, while synchrotron self-Compton scattering can explain the observed γ-rays. Applying the inhomogeneous relativistic jet model, the derived value of the magnetic field is similar to the X-ray bright BL Lac object Mrk 421 and higher than for the OVV quasar 3C 279. The spectral hardening with increasing intensity in PKS 2005−489 can be accounted for by a small gradient in the density of relativistic electrons and by a substantial increase of their maximum energy. We suggest that magnetic field strengths and particle energies may be the main physical quantities governing the shape of the multifrequency continuum emission in blazars.

R. M. S. acknowledges financial support from NASA grant NAG5-1918. We thank Paolo Giommi for a useful referee report. This research has made use of the NASA/IPAC Extragalactic Database (NED) which is operated by the Jet Propulsion Laboratory, California Institute of Technology, under contract with the National Aeronautics and Space Administration.

REFERENCES

Bersanelli, M., Bouchet, P., Falomo, R., & Tanzi, E. G. 1992, AJ, 104, 28
Briel, U. G., et al. 1994, The *ROSAT* Users' Handbook, in preparation
Brinkmann, W., & Siebert, J. 1994, A&A, 285, 812
Canizares, C. R., & Kruper, J. 1984, ApJ, 278, L99
Dermer, C., Schlickeiser, R., & Mastichiadis, A. 1992, A&A, 256, L27
Dondi, L., & Ghisellini, G. 1995, MNRAS, in press
Edelson, R., Pike, G. F., Saken, J. M., Kinney, A., & Shull, J. M. 1992, ApJS, 83, 1
Edge, A. C., & Stewart, G. C. 1991, MNRAS, 252, 428
Falomo, R., Bersanelli, M., Bouchet, P., & Tanzi, E. G. 1993, AJ, 106, 11
Falomo, R., Maraschi, L., Tanzi, E. G., & Treves, A. 1987, ApJ, 318, L39
Fruscione, A. 1995, in preparation
George, I. M., Warwick, R. S., & Bromage, G. E. 1988, MNRAS, 232, 793
Giommi, P., Ansari, S., & Micol, A. 1995, A&AS, 109, 267
Giommi, P., Barr, P., Garilli, B., Maccagni, D., & Pollack, A. M. T. 1990, ApJ, 356, 432
Giommi, P., & Padovani, P. 1994, MNRAS, 268, L51
Ghisellini, G., & Maraschi, L. 1994, in The Second Compton Symposium, ed. C. E. Fichtel, N. Geherels, & J. P. Norris (New York: AIP), 616
Ghisellini, G., Maraschi, L., & Treves, A. 1985, A&A, 146, 204
Königl, A. 1989, in BL Lac Objects, ed. L. Maraschi, T. Maccacaro, & M.-H. Ulrich (Berlin: Springer), 321
Krolik, J. H., Kallman, T. R., Fabian, A. C., & Rees, M. J. 1985, ApJ, 295, 104
Kühr, H., Witzel, A., Pauliny-Thoth, I. I. K., & Nauber, U. 1981, A&AS, 45, 367
Impey, C. D., & Neugebauer, G. 1988, AJ, 95, 307
Large, M. I., Mills, B. Y., Little, A. G., Crawford, D. F., & Sutton, J. M. 1981, MNRAS, 194, 1013
Ledden, J. E., & O'Dell, S. L. 1985, ApJ, 298, 630
Madejski, G. M., et al. 1995, ApJ, 438, 672
Maraschi, L., et al. 1994, ApJ, 435, L91
Maraschi, L., Ghisellini, G., & Boccasile, A. 1994, in The Nature of Compact Objects in AGNs, ed. A. Robinson & R. J. Terlevich (Cambridge: Cambridge Univ. Press), 381

Maraschi, L., Ghisellini, G., & Celotti, A. 1992, ApJ, 397, L5
Maraschi, L., Ghisellini, G., Tanzi, E. D., & Treves, A. 1986, ApJ, 310, 325
Marshall, H. L., Fruscione, A., & Carone, T. E. 1995, ApJ, 439, 90
Pesce, J. E., Falomo, R., & Treves, A. 1994, AJ, 107, 494
Price, R., Burns, J. O., Durie, N., & Newberry, M. V. 1991, AJ, 102, 14
Sambruna, R. M., Barr, P., Giommi, P., Maraschi, L., Tagliaferri, G., & Treves, A. 1994a, ApJ, 434, 468
———. 1994b, ApJS, 95, 371
Sambruna, R. M., et al. 1995, in preparation
Savage, A., Bolton, J. G., & Wright, A. E. 1977, MNRAS, 179, 135
Sembay, S., et al. 1993, ApJ, 404, 112
Sikora, M., Begelman, M. C., & Rees, M. J. 1994, ApJ, 421, 153
Stark, A. A., Gammie, C. F., Wilson, R. W., Bally, J., Linke, R. A., Heiles, C., & Hurwitz, M. 1992, ApJS, 79, 77
Stickel, M., Padovani, P., Urry, C. M., Fried, J. W., & Kühr, H. 1991, ApJ, 374, 431
Urry, C. M., et al. 1995, in preparation
Wall, J. V., Danziger, I. J., Pettini, M., Warwick, R. S., & Wamsteker, W. 1986, MNRAS, 219, 23P
Wall, J. V., Shimmins, A. J., & Bolton, J. G. 1975, Australian J. Phys., Astrophys. Suppl., No. 34, 55
White, N. E., Giommi, P., & Angelini, L. 1994, BAAS, 26, 1372